Original Article

Right ventricular volume-strain loops using 3D echocardiography-derived mesh models: proof-of-concept application on patients undergoing different types of open-heart surgery

Marius Keller^, Ann-Sophie Puhlmann, Tim Heller, Peter Rosenberger, Harry Magunia^

Department of Anesthesiology and Intensive Care Medicine, University Hospital Tuebingen, Eberhard-Karls-University, Tuebingen, Germany

Contributions: (I) Conception and design: M Keller, H Magunia; (II) Administrative support: P Rosenberger, H Magunia; (III) Provision of study materials or patients: M Keller, P Rosenberger, H Magunia; (IV) Collection and assembly of data: M Keller, AS Puhlmann, T Heller, H Magunia; (V) Data analysis and interpretation: M Keller, AS Puhlmann, T Heller, H Magunia; (VI) Manuscript writing: All authors; (VII) Final approval of manuscript: All authors.

Correspondence to: Dr. Marius Keller. Department of Anesthesiology and Intensive Care Medicine, University Hospital, Hoppe-Seyler-Str. 3, 72076 Tuebingen, Germany. Email: marius.keller@med.uni-tuebingen.de.

Background: Right ventricular (RV) function can be quantified by right heart catheterization-derived pressure-volume loops. While this technique is invasive, echocardiography-based volume-strain loops (VSLs) potentially reflect a non-invasive alternative. In this study, an approach to generate VSLs from volume and multidimensional strain data of 3D echocardiography-derived RV mesh models is evaluated with regard to feasibility and reproducibility.

Methods: In a retrospective cohort study design, 3D intraoperative transesophageal echocardiograms of twenty-three patients undergoing aortic valve surgery (AVS) and eighteen patients undergoing off-pump coronary artery bypass (OPCAB) grafting were available prior to sternotomy and after sternal closure. RV meshes were generated using 3D speckle-tracking. Custom-made software quantified the meshes' volumes, global longitudinal (RV-GLS) and global circumferential strain (RV-GCS) for VSL generation. Linear regression of systolic VSLs yielded slopes, intercepts and systolic areas. Polynomial regression of two orders was used to analyze systolic-diastolic coupling at 10% increments of the RV end-diastolic volume (RVEDV). Reproducibility was analyzed by fourfold double-measurements of four datasets.

Results: VSL calculation was feasible from all included 3D datasets. RV-GLS remained unaltered, but RV-GCS worsened in AVS [abs. diff. (Δ) 3.9%, P<0.01] and OPCAB patients (Δ4.5%, P<0.001). While RV-GCS systolic areas were markedly reduced at the end of AVS (Δ268mL%, P<0.01) and OPCAB (Δ185mL%, P<0.001), RV-GCS slopes did not change. Systolic-diastolic uncoupling was not observed, but in trend, decreased diastolic RV-GCS after AVS (P=0.06) and increased diastolic RV-GCS after OPCAB (P=0.06) were observed. Intraclass correlation coefficients (0.84–0.98) and coefficients of variation (6.4–11.8%) indicated good reproducibility.

Conclusions: RV VSL generation using 3D echocardiography-derived mesh models is feasible. Longitudinal and circumferential strain vectors yield intrinsically different VSL indices. In future investigations, VSLs of multidimensional strains could provide further insight into periprocedural changes of RV mechanics.

^ ORCID: Harry Magunia, 0000-0001-9576-6399; Marius Keller, 0000-0002-5810-8845.

Keywords: Three-dimensional echocardiography; right ventricle; volume-strain loops; cardiac surgery

Submitted Dec 14, 2021. Accepted for publication Mar 28, 2022.
doi: 10.21037/qims-21-1204
View this article at: https://dx.doi.org/10.21037/qims-21-1204

Introduction

The quantification of right ventricular (RV) systolic function is cornerstone to identify RV dysfunction which dramatically limits patient outcomes (1-3). The delineation between normal and reduced RV function is challenging, and certainly depends on the clinical setting. Echocardiography has emerged as the first-line diagnostic tool for RV assessment, mainly due to its rapid availability and non-invasiveness (4,5). Three-dimensional (3D) techniques provide a comprehensive display of the anatomically complex RV compared to the reference method cardiac magnetic resonance imaging (6) and have the potential to identify hallmarks of RV deterioration (7,8). Semi-automatic speckle-tracking echocardiography (STE) and strain analyses recently expanded the spectrum of RV characterization by 3D echocardiography (9,10). As most echocardiographic parameters depend on pre- and afterload, right heart catheterization-based measurements—especially pressure-volume relationships—reflect advantageous techniques for the quantification of RV contractility and diastolic function (11). However, right heart catheterization is invasive and conductance catheter-based volumetry often cumbersome (12,13). Accordingly, the acquisition of pressure-volume loops is mostly withheld from patients in clinical routine but plays a pivotal role in scientific contexts (14,15). Volume-strain or area-strain loops were evaluated as a potential non-invasive correlate of pressure-volume loops over the last years and approaches to generate RV load-strain loops yielded promising results (16,17). Volume-strain loops (VSLs) describe the change of RV deformation across the cardiac cycle for a defined volume change and—similarly to pressure-volume loops—various systolic and diastolic parameters can be derived, e.g., slopes of the VSL curve (18). Changes in RV pre- or afterload detected by simultaneous recordings of strain and volume correlate well with pressure-volume loops (16). So far, a limitation of these techniques was the character of the input parameters (area/volume, strain), which were either derived from two-dimensional echocardiograms or underwent necessary interpolation due to unsynchronized recordings. To the best of our knowledge, this report incorporates the first approach to generate non-invasive real-time VSLs employing volume and strain data extracted from a single 3D echocardiographic dataset. The application of 3D STE on intraoperative transesophageal echocardiograms yielded RV mesh models that underwent post-processing with custom-made software to derive volume and strain values simultaneously for each frame of the cardiac cycle. The goal of this proof-of-concept study was to evaluate the feasibility of 3D VSLs in patients undergoing two different types of cardiac procedures, and to analyze their periprocedural changes alongside other established echocardiographic parameters. We present the following article in accordance with the STROBE reporting checklist (available at https://qims.amegroups.com/article/view/10.21037/qims-21-1204/rc).

Methods

Patients, interventions & echocardiography

In this single-center observational retrospective cohort study, patients undergoing cardiac surgery were chosen from our institutional echocardiographic imaging database. The study was conducted in accordance with the Declaration of Helsinki (as revised in 2013) and approved by the Ethics Committee of the University of Tuebingen (Trial Registration # IRB 350/2015R). German privacy regulations do not require individual patient consent for retrospective data acquisition or use. Out of 738 patients in the 3D database eligible between November 2013 and October 2018, twenty-three patients that underwent on-pump surgery of the aortic valve (AVS: replacement or repair) and eighteen patients that underwent off-pump coronary artery bypass (OPCAB) grafting were included due to the necessary echocardiograms being available (*Figure 1*). The two patient groups were chosen for the following reasons: (I) after screening of the database, AVS and OPCAB patients represented the two surgical procedure groups with the most patients suitable for inclusion; (II) RV physiology of AVS and OPCAB patients is intrinsically different (AVS: increased afterload, on-pump surgery; OPCAB: myocardial ischemia, off-pump surgery) leading to a higher probability to detect characteristic changes of VSLs between the groups or between the pre- and postoperative

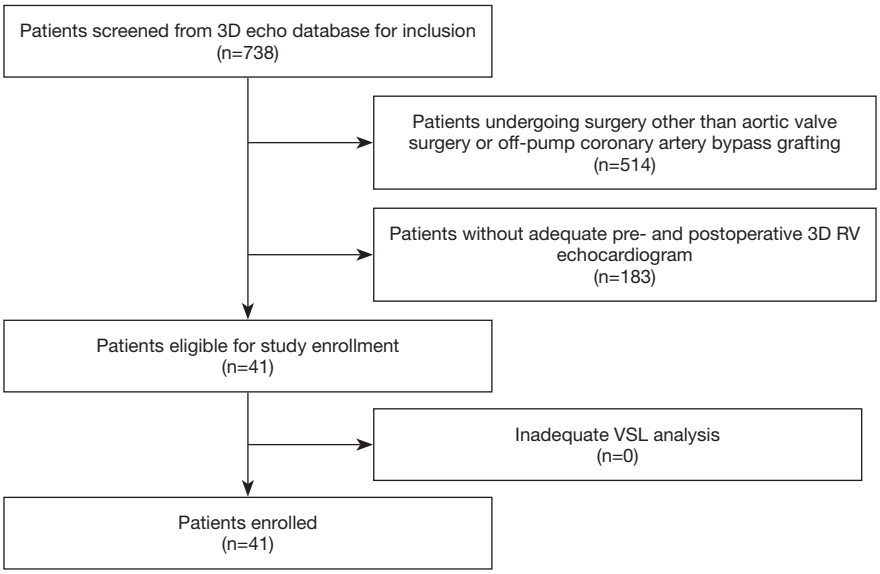

Figure 1 Patient selection flow chart. Patients were screened for study inclusion by searching the institutional 3D echocardiography database. VSL generation was feasible in all included patients. RV, right ventricular; VSL, volume-strain loop.

state. All included patients received standardized 3D TEE during hemodynamic stability under general anesthesia both prior to sternotomy ("pre") and after sternal closure ("post"). The institutional protocol for intraoperative 3D TEE acquisition has been extensively described elsewhere (19-22). In brief, a RV-focused 3D recording was performed using multi-beat acquisition to achieve sufficient frame rates for STE-based volumetry (*Figure 2A*). Perioperative pacing was read out from digital intraoperative records.

Post-processing, mesh generation & recording of volume-strain loops

The 3D datasets were segmented using the most widespread commercially available software package (4D RV-Function 2, Tomtec Imaging Systems GmbH, Unterschleissheim, Germany, *Figure 2A*). After global RV volumetric parameters were recorded (RVEDV, RVESV, RVEF), the meshes were exported and analyzed with a custom-made software (written in C++. based on the Visualization Toolkit, Ver. 7.1.1, Kitware, Inc., Clifton Park, New York, USA). This algorithm quantifies the mesh volume and strains on the mesh surface from frame to frame (*Figure 2B*). Strain computation using this software approach and its prognostic value have recently been described (22,23): in the present study, right ventricular global longitudinal strain (RV-GLS) was calculated by averaging two regional longitudinal strains, each of them running from the tricuspid valve to the apex (reflecting free wall and septal wall longitudinal strain). Right ventricular global circumferential strain (RV-GCS) was quantified by averaging four regional circumferential strains (basal upper, basal lower, apical upper and apical lower circumferential strain). As volumetric and strain data are available simultaneously in each frame of the cardiac cycle, no interpolations or merging of volume and strain curves from different modalities are necessary. A spreadsheet of the raw data is written by the software (*Figure 2C*) and the volume-strain loop is generated using Microsoft Excel (*Figure 2D*). The largest and smallest mesh volumes were defined as the end-diastolic and end-systolic frame, respectively. Systolic and diastolic volume-strain relationships were calculated and displayed separately. Peak strain values (of the whole cardiac cycle) were recorded for the comparisons with VSL parameters.

Calculation of VSL parameters

Linear regression yielded equations in the form of $y = m \times x + z$ for systolic volume-strain relationships separately for RV-GLS and RV-GCS, respectively [y = strain (%), m = slope (%/mL), x = volume (mL), z = intercept (%)]. The area under the curve in systolic volume-strain relationships was calculated for RV-GLS and RV-GCS, respectively, and termed "systolic area" (mL*%). Systolic and diastolic

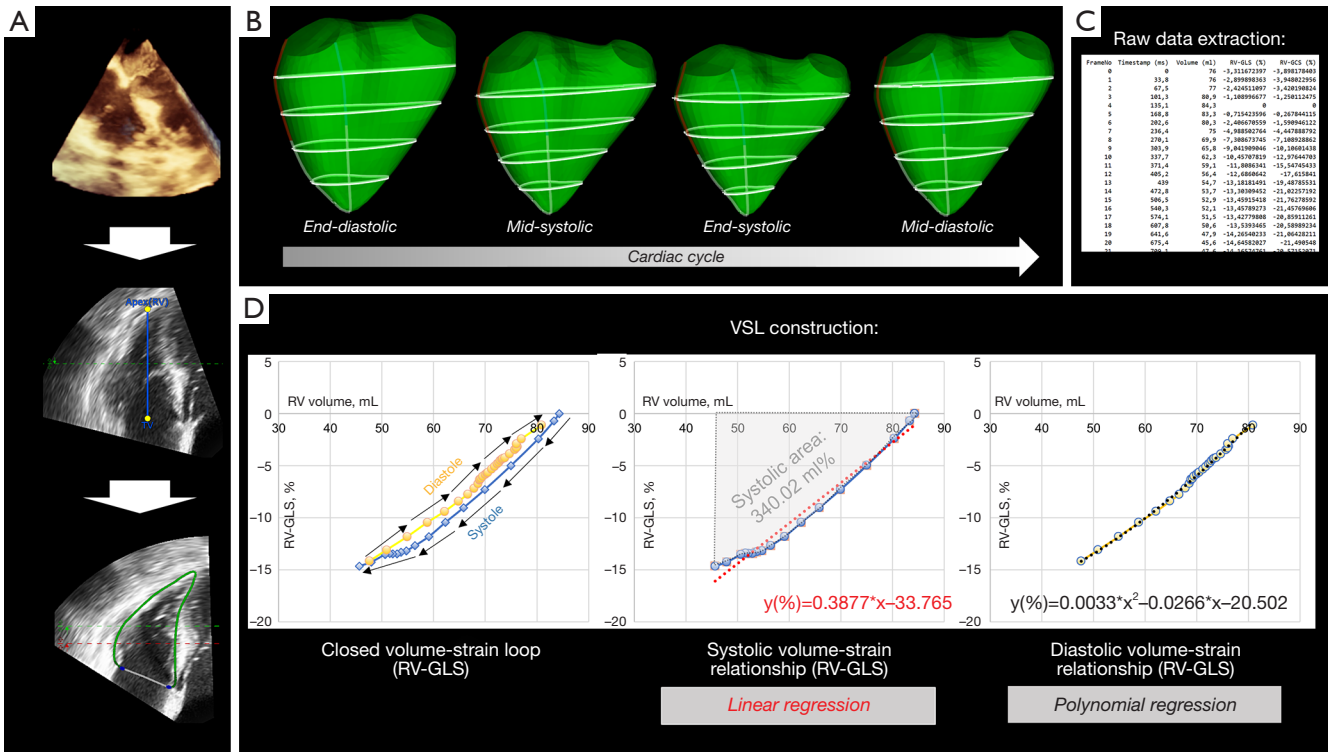

Figure 2 Generation of RV VSLs using simultaneously recorded volume and strain data from 3D speckle-tracking echocardiography-derived mesh models. (A) Offline segmentation and semi-automatic endocardial border detection of 3D echocardiographic RV studies using speckle-tracking. (B) The generated mesh models undergo volume and strain analysis (right ventricular global circumferential strain "RV-GCS" and right ventricular global longitudinal strain "RV-GLS") of the whole cardiac cycle employing a custom-made software. (C) Volumetric and strain data are generated frame-by-frame and exported into a raw data file. (D) VSLs are constructed for the whole cardiac cycle (closed VSL) as well as for the systolic and diastolic phases separately. Exemplary display of a linear regression model of the systolic volume-strain relationship (red dotted line) and a polynomial regression model of the diastolic volume-strain relationship (black dotted line), respectively. RV, right ventricular; VSLs, volume-strain loops; RV-GCS, right ventricular global circumferential strain; RV-GLS, right ventricular global longitudinal strain.

components further underwent polynomial regression of two orders ($y = k_1 \times x^2 + k_2 \times x + k_3$) separately. These equations were used to compute ideal strain values at 10% increments of the RVEDV between 100% and 50%, resulting in a normalized RVEF of 50%. The difference at each 10% increment between systolic and diastolic strains (Δsys-dia) was referred to as "systolic-diastolic coupling" according to the method of Oxborough *et al.* (17). Systolic-diastolic uncoupling was present by definition if ideal systolic and diastolic strains differed significantly at a given 10% increment of the RVEDV.

Reproducibility analysis

To investigate the reproducibility of mesh-derived VSL parameters, four 3D echocardiographic datasets were randomly picked from the study cohort. Three additional mesh models were generated from each of the 3D studies in addition to the initial meshes, resulting in four total mesh models per dataset. Two-way mixed intraclass correlation coefficients (ICCs) for absolute agreement on average measurements and the average of the coefficients of variation were calculated for slopes, intercepts and systolic areas of RV-GLS and RV-GCS VSLs, respectively.

Statistical analysis

Normally distributed continuous variables are presented as the mean ± standard deviation while nonnormally distributed continuous variables are presented as the median

Table 1 Baseline characteristics of the study population

Parameter	AVS (n=23)	OPCAB (n=18)	P value	MD 95% CI
Age (years)	62.2±8.2	69.0±9.8	0.92	−6.0 to 5.4
Male	15 [65]	14 [78]	0.57	−18 to 40
BMI (kg/m²)	29.6±4.6	29.9±7.0	0.86	−3.6 to 4.3
eGFR (mL/min)	92.0±30.4	71.5±30.7	0.04*	−39.9 to −1.1
LVEF <50%	8 [35]	8 [44]	0.79	−23 to 40
NYHA class > II	14 [61]	7 [39]	0.28	−12 to 51
IDDM	3 [13]	6 [33]	0.25	−9 to 48
Chronic lung disease	5 [22]	3 [17]	0.99	−24 to 31

Values are means ± standard deviations or proportions [percentages]. Unpaired Student's *t*-tests and chi-squared tests were used to calculate P values. *, P<0.05. AVS, aortic valve surgery; BMI, body mass index; CI, confidence interval; eGFR, estimated glomerular filtration rate; IDDM, insulin-dependent diabetes mellitus; LVEF, left ventricular ejection fraction; MD, mean difference; NYHA, New York Heart Association; OPCAB, off-pump coronary artery bypass grafting.

Table 2 3D echocardiographic data from before sternotomy (pre) and after sternal closure (post)

Parameter	Pre	Post	P value	MD 95% CI
Aortic valve surgery (n=23)				
RVEDV (mL)	149±45	140±48	0.16	−21 to 4
RVESV (mL)	84±30	86±33	0.69	−8 to 11
RVEF (%)	44±7	39±11	0.03*	−10 to −1
RV-GLS (%)	−18.2±4.1	−16.6±5.2	0.14	−0.6 to 3.8
RV-GCS (%)	−19.4±3.6	−15.5±6.2	<0.01**	1.2 to 6.7
Off-pump coronary artery bypass grafting (n=18)				
RVEDV (mL)	139±31	138±34	0.86	−15 to 13
RVESV (mL)	78±21	85±26	0.22	−4 to 18
RVEF (%)	44±6	39±6	0.01*	−9 to −1
RV-GLS (%)	−17.9±4.3	−15.3±3.6	0.05	−0.1 to 5.3
RV-GCS (%)	−19.3±4.0	−14.8±3.4	<0.001***	2.2 to 6.8

Values are means ± standard deviations. Paired Student's t-tests were used to calculate P values. *, P<0.05; **, P<0.01; ***, P<0.001. CI, confidence interval; MD, mean difference; RV-GCS, right ventricular global circumferential strain; RV-GLS, right ventricular global longitudinal strain; RVEDV, right ventricular end-diastolic volume; RVEF, right ventricular ejection fraction; RVESV, right ventricular end-systolic volume.

(interquartile range). Comparisons were performed with unpaired/paired Student's *t*-tests for normally distributed continuous variables, Wilcoxon tests for nonnormally distributed continuous variables and Chi-squared tests for proportions. The significance level was set at P<0.05. Significant P values were highlighted as follows: <0.05*, <0.01**, <0.001***.

Results

Mesh generation was possible from all included 3D datasets (n=82) and VSL analysis was feasible in 100% of these meshes. Baseline patient characteristics are given in *Table 1*. *Table 2* gives an overview of the study groups' 3D echocardiographic RV data before and after the interventions. In the AVS group, 14/23 patients (61%)

Table 3 Parameters derived from systolic volume-strain relationships before sternotomy (pre) and after sternal closure (post)

Parameter	Pre	Post	P value	MD 95% CI
Aortic valve surgery (n=23)				
RV-GLS				
Slope m (%/mL)	0.29±0.10	0.33±0.13	0.04*	0.00 to 0.08
Intercept z (%)	−38.8±6.6	−40.9±8.6	0.39	−2.9 to 7.2
Systolic area (mL*%)	459 [392–619]	410 [279–522]	0.02*	–
RV-GCS				
Slope m (%/mL)	0.31±0.11	0.32±0.19	0.91	−0.06 to 0.07
Intercept z (%)	−43.1±6.0	−37.8±13.1	0.06	−10.7 to 0.2
Systolic area (mL*%)	616 [471–761]	348 [252–549]	<0.01**	–
Off-pump coronary artery bypass grafting (n=18)				
RV-GLS				
Slope m (%/mL)	0.30±0.11	0.30±0.09	0.87	−0.06 to 0.05
Intercept z (%)	−38.5±6.0	−37.9±8.0	0.77	−5.3 to 4.1
Systolic area (mL*%)	481 [415–577]	390 [288–467]	<0.01**	–
RV-GCS				
Slope m (%/mL)	0.33±0.10	0.29±0.09	0.07	−0.09 to 0.00
Intercept z (%)	−43.7±5.9	−36.8±7.2	<0.001***	−9.0 to −2.9
Systolic area (mL*%)	554 [427–651]	369 [292–439]	<0.001***	–

Values are means ± standard deviations or medians (interquartile range). Paired Student's *t*-tests were used to calculate P values for normally distributed samples, Wilcoxon tests were used in cases of non-normal distribution. *, P<0.05; **, P<0.01; ***, P<0.001. CI, confidence interval; MD, mean difference; RV-GCS, right ventricular global circumferential strain; RV-GLS, right ventricular global longitudinal strain.

required epicardial AAI pacing after weaning from CPB (90–100 beats per minute), but no AV blocks or ventricular pacing was present at any time throughout surgery. No OPCAB patient was paced perioperatively. RVEF and RV-GCS deteriorated significantly in the AVS and OPCAB group, respectively. RV-GLS was also reduced in both groups at the end of the procedure, but the differences did not reach significance. Systolic VSL parameters (slopes, intercepts and systolic areas) are displayed in *Table 3*. Significant changes of slopes or intercepts between pre- and postoperative values were only found sporadically. While RV-GLS slopes increased in the AVS patients, RV-GCS intercepts decreased in value in the OPCAB group. Strikingly, systolic areas decreased significantly for RV-GLS and RV-GCS in both patient groups. The analyses of ideal strain values at 10% increments of the RVEDV are shown in *Figure 3* and *Table 4*. Statistically, no systolic-diastolic uncoupling was observed with regard to patient group, time point or strain direction.

Table 5 lists the results of the reproducibility analysis employing the repeated VSL calculations (n=4) from the 3D echocardiograms of four patients. High ICCs indicated satisfying reproducibility of slopes, intercepts and systolic areas, respectively. Except for RV-GLS slopes (11.8%), coefficients of variations were lower than 10%.

Discussion

Study goals & perioperative implications

The results of the present proof-of-concept study clearly demonstrate that RV VSL generation from 3D STE-derived mesh models is feasible and reproducible. The investigated study cohort consisted of patients under

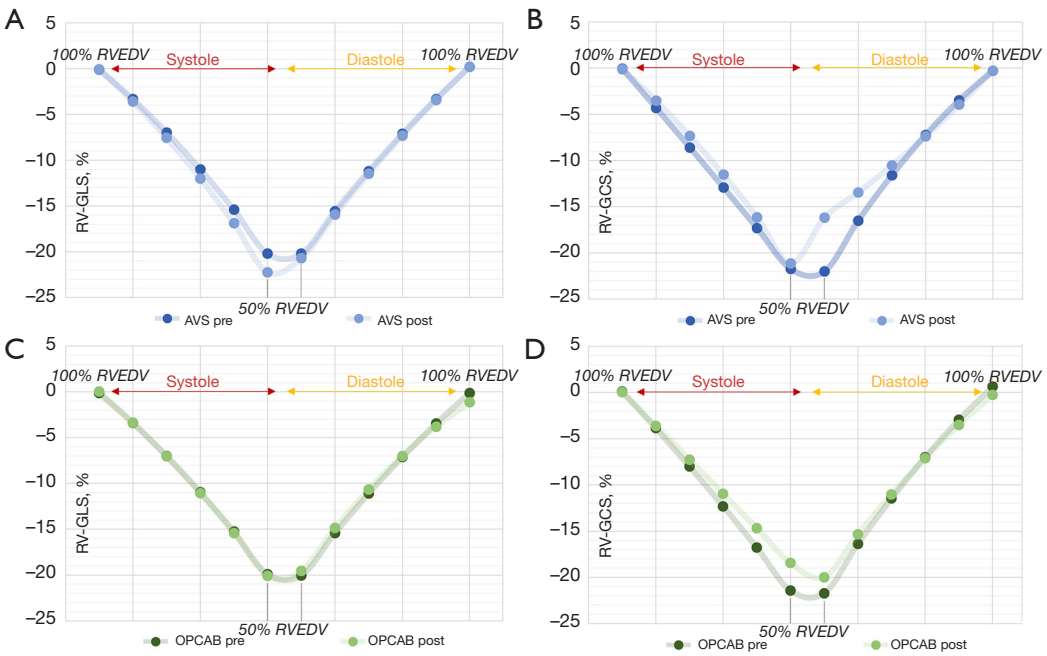

Figure 3 Systolic and diastolic ideal strain calculation using polynomial regression at 10% increments of the RVEDV within a normalized RVEF range of 50%. Patients undergoing aortic valve surgery (AVS, A+B) and off-pump coronary artery bypass grafting (OPCAB, C+D) show no significant alterations between "pre" (before sternotomy) and "post" (after sternal closure) recordings of right ventricular global longitudinal strain (RV-GLS, A+C). For right ventricular global circumferential strain (RV-GCS, B+D), the curves of the AVS patients (dark blue and light blue) point to new-onset early systolic-diastolic uncoupling after the procedure (Δsys-dia =−5.0%±12.0% at 50% increment of the RVEDV, P=0.06). RVEDV, right ventricular end-diastolic volume; RVEF, right ventricular ejection fraction; OPCAB, off-pump coronary artery bypass; RV-GLS, right ventricular global longitudinal strain; AVS, aortic valve surgery; RV-GCS, right ventricular global circumferential strain.

Table 4 Ideal strain calculations and systolic-diastolic coupling analysis using polynomial regression of the volume-strain relationships

Parameter	RV-GLS		RV-GCS	
	Pre	Post	Pre	Post
Aortic valve surgery (n=23)				
Systolic strain, %				
90% RVEDV	−3.3±1.1	−3.6±1.1	−4.3±1.1	−3.5±1.8
80% RVEDV	−7.0±1,7	−7.6±2.0	−8.6±1.7	−7.3±3.1
70% RVEDV	−11.0±2.1	12.0±3.4	−12.9±1.9	−11.5±4.2
60% RVEDV	−15.4±2.7	−16.9±5.9	−17.3±2.2	−16.1±5.4
50% RVEDV	−20.2±3.6	−22.2±9.5	−21.7±3.3	−21.1±7.1
Diastolic strain, %				
90% RVEDV	−3.3±1.0	−3.4±1.3	−3.5±1.0	−3.9±1.1
80% RVEDV	−7.1±1.7	−7.3±2.0	−7.2±1.5	−7.4±2.1
70% RVEDV	−11.2±2.2	−11.5±2.6	−11.6±2.0	−10.5±4.0

Table 4 (*continued*)

Table 4 (*continued*)

Parameter	RV-GLS		RV-GCS	
	Pre	Post	Pre	Post
60% RVEDV	−15.6±2.8	−15.9±3.3	−16.5±2.5	−13.5±7.3
50% RVEDV	−20.2±3.6	−20.7±4.7	−22.0±3.4	−16.2±12.1
Systolic-diastolic coupling (Δsys-dia), %				
90% RVEDV	0.0±1.2	−0.2±1.1	−0.8±1.3	0.4±1.5
80% RVEDV	0.1±1.4	−0.2±1.4	−1.3±1.8	0.0±2.4
70% RVEDV	0.2±1.1	−0.5±1.9	-1.3±1.6	−1.0±3.8
60% RVEDV	0.2±0.8	−0.9±3.9	−0.8±1.2	−2.7±6.9
50% RVEDV	0.0±2.4	−1.6±7.2	−0.2±2.7	−5.0±12.0
Off-pump coronary artery bypass grafting (n=18)				
Systolic strain, %				
90% RVEDV	−3.4±0.9	−3.3±0.6	−3.8±1.2	−3.6±1.1
80% RVEDV	−7.0±1.4	−7.0±1.3	−8.0±1.7	−7.3±1.8
70% RVEDV	−10.9±1.8	−11.1±2.2	−12.3±2.0	−11.0±2.3
60% RVEDV	−15.3±2.2	−15.4±3.6	−16.8±2.3	−14.7±3.2
50% RVEDV	−19.9±2.8	−20.1±5.4	−21.4±3.0	−18.4±4.8
Diastolic strain, %				
90% RVEDV	−3.5±0.9	−3.8±2.1	−2.9±1.6	−3.5±1.5
80% RVEDV	−7.1±1.1	−7.0±1.8	−7.0±1.5	−7.1±1.6
70% RVEDV	−11.1±1.5	−10.7±2.8	−11.5±1.9	−11.0±2.4
60% RVEDV	−15.4±2.0	−14.9±4.1	−16.4±2.2	−15.3±3.9
50% RVEDV	−20.0±2.8	−19.5±6.3	−21.7±2.6	−20.0±6.3
Systolic-diastolic coupling (Δsys-dia), %				
90% RVEDV	0.1±1.1	0.5±1.9	−0.9±1.9	−0.1±1.5
80% RVEDV	0.1±1.2	0.0±1.2	−1.0±2.2	−0.2±1.1
70% RVEDV	0.2±1.1	−0.4±1.1	−0.8±2.0	0.1±1.1
60% RVEDV	0.2±1.0	−0.6±1.1	−0.4±1.3	0.7±1.6
50% RVEDV	0.1±1.5	−0.5±2.9	0.3±1.3	1.6±3.2

Values are means ± standard deviations. Systolic and diastolic strains at 10% increments of the RVEDV were compared with paired Student's *t*-test. Post, under general anesthesia after sternal closure; pre, under general anesthesia and before sternotomy; RV-GCS, right ventricular global circumferential strain; RV-GLS, right ventricular global longitudinal strain; RVEDV, right ventricular end-diastolic volume.

general anesthesia, receiving TEEs before and after open-heart surgery. In between examinations, one group underwent AVS including cardiopulmonary bypass (CPB) and the second group underwent OPCAB grafting. In both groups, RVEF and RV-GCS were markedly reduced at the end of surgery. Postoperative reductions of RV systolic function or morphological switches of the contraction pattern as a response to inflammation, CPB or surgical stress have been reported and discussed intensively (24-27). However, the influence of factors associated with open-

Table 5 Reproducibility of VSL-derived systolic parameters

Parameter	ICC (95% CI)	VC (%)
RV-GLS		
Slope m	0.97 (0.85–1.00)	11.8
Intercept z	0.84 (0.22–0.99)	9.0
Systolic area	0.98 (0.92–1.00)	9.1
RV-GCS		
Slope m	0.98 (0.92–1.00)	9.3
Intercept z	0.95 (0.76–1.00)	6.4
Systolic area	0.98 (0.88–1.00)	7.6

VSL, volume-strain loop; ICC, intraclass correlation coefficient; CI, confidence interval; RV-GLS, right ventricular global longitudinal strain; RV-GCS, right ventricular global circumferential strain; VC, coefficient of variation (average).

heart surgery on RV function remains unclear, and assumptions on intrinsically reduced RV contractility or diastolic function require scientific proof. As only a fraction of AVS patients were paced in AAI mode postoperatively and no ventricular pacing was present in any patients, a significant influence of pacing on the RV contraction pattern is unlikely.

Possible correlations between VSL indices and invasive parameters

The analysis of the volume-strain relationship might facilitate our understanding of perioperative alterations of RV function, and differentiate between adaptions and deteriorations. Whether the slopes of the systolic volume-strain relationships share properties with the slopes of the end-systolic pressure-volume relationships, and consequently serve as a non-invasive single-beat measure of myocardial contractility, can only be assumed (16). If so, however, it is remarkable that VSL slopes showed no systematic procedure-related reductions in AVS or OPCAB patients. Strikingly, systolic areas—the systolic volume-strain integrals—were dramatically reduced in both groups at the end of the procedure, potentially reflecting a correlate of myocardial work of the corresponding strain vector (longitudinal or circumferential). A clear weakness of the systolic area is the presumable afterload dependence, which cannot be considered due to the lack of the variable "pressure". Interpretation of the intercept is even less trivial: the intercept represents the hypothetical peak strain value that is generated by a complete emptying of the RV (an ejection fraction of 100% using the linear regression model) in its current hemodynamic state, regarding pre- and afterload. While RV-GLS intercepts remained unaltered in both patient groups, RV-GCS intercepts decreased significantly in OPCAB patients and in trend in AVS patients (P=0.06). The intercepts depend on RV volumes and slope, but neither was significantly altered in the patient groups. The nature of the increments makes a correlation with RV preload and diastolic filling pressures possible, but this needs to be investigated in future studies (RVEDV did not change during the procedures).

Systolic-diastolic coupling analysis

Regarding the VSL-based analysis of systolic-diastolic coupling, deriving systolic and diastolic polynomial regression models and standardizing strains to the individual's RVEDV revealed an absence of statistically significant systolic-diastolic uncoupling in our patients. However, the graphical displays revealed two phenomena: (I) after OPCAB, ideal diastolic RV-GCS values (at 50% RVEDV) were higher in value than their systolic counterparts (Δsys-dia 1.6%±3.2%, P=0.06), potentially reflecting increased early and mid-diastolic relaxation velocities. Optimizing myocardial oxygenation through the restoration of coronary blood flow, leading to an immediate improvement of diastolic function could serve as an explanation (28), especially since 9 of the 18 OPCAP patients (50%) underwent right coronary revascularization. (II) Ideal RV-GCS curves showed a dissociation of systolic and diastolic strain values at 50% RVEDV after AVS. While the difference was not significant (Δsys-dia −5.0%±12.0%, P=0.06), it points towards systolic-diastolic uncoupling, particularly considering the small number of included patients. Early diastolic dysfunction after CPB-related cardioplegia, ischemia and reperfusion has been observed (29,30) and might be reflected by VSL-derived Δsys-dia. Naturally, Δsys-dia needs to be compared to conventional strategies for the assessment of diastolic function in future studies.

RV mechanics & load-strain relationships (volume or area)

Literature on the perioperative changes of RV mechanics following cardiac surgery is conflicting. While the effects presumably depend on the procedure, comorbidities and other perioperative variables (such as the use of CPB), most studies report a reduction of RV longitudinal function

while global RV function is maintained (19,24,27,31-33). However, systematic assessment of RV mechanics employing 3D echocardiography is only used in a limited number of these investigations, potentially underestimating the role of circumferential RV function. Interestingly, a study by Lakatos *et al.* using a novel 3D STE-based technique to quantify the relative contributions of different RV motion components found that circumferential contraction contributes significantly more to RV stroke volume ejection than the longitudinal component (34).

In support of these findings, Oxborough *et al.* were able to differentiate the RV mechanical pattern of high endurance athletes from control subjects using longitudinal area-strain loops (17): while absolute peak strains did not differ between the groups, ideal longitudinal strains at 10% increments of the end-diastolic area were significantly smaller in value in the athlete group. The authors attribute this to a potential increase of circumferential reserve at rest to which the longitudinal area-strain relationship is blind. Nevertheless, published data on longitudinal volume-strain or area-strain relationships provide insight into the transduction of RV functional changes into VSL-derived parameters. The slopes of 2D longitudinal systolic area-strain loops were recently shown to be predictors of long-term survival in patients with pulmonary hypertension (18). Works from the same group demonstrate a correlation between systolic slopes and afterload, reflected by invasively determined pulmonary vascular resistance (35). With regard to preload, an increase or a reduction of venous return to the right atrium led to a paradoxical response in the longitudinal systolic slope of healthy subjects (where a preload increase causes a reduction of the slope and vice versa) (16). Again, this might reflect a shift towards circumferential contraction with increased EDVs, which can only be addressed when circumferential VSL parameters are available. This limitation could presumably be overcome with the presented mesh-derived method of simultaneous longitudinal and circumferential VSL generation in future investigations. A recent approach to quantify indices of right ventricular myocardial work by non-invasive echocardiography-derived pressure-strain loops revealed significant associations with right heart catheterization-based measurements (36). As conventional echocardiographic parameters showed no correlation with invasive RV pressure-volume loops, the non-invasive assessment of RV myocardial work might enhance the diagnostic spectrum in the near future. Besides reflecting a non-invasive alternative to pressure-volume loops, 3D-derived VSLs could carry additional value for the detection of early RV dysfunction, the initiation of hemodynamic therapies and the guidance of postoperative ICU regimens. Overall, the age of right ventricular volume-strain loops is still young, and a high number of profound studies will help to facilitate the decryption of RV pathologies using VSLs and drive clinical implementation of the applied techniques. STE-based generation of RV meshes is feasible in under 5 minutes (22) and all following processes for VSL calculation can be fully automatized, potentially enabling future bedside application and rapid clinical decision-making.

Limitations

This was an exploratory single-center study, primarily investigating merely the technical feasibility of volume-strain loop generation from simultaneously recorded 3D echocardiography input data. The number of patients retrospectively included is very small. Despite echocardiographic image quality having no impact on patient selection, the small percentage of patients retrospectively included from a large database may potentially be associated with a risk for inclusion bias. All measurements were performed under general anesthesia, limiting the applicability of the results on awake and spontaneously breathing patients. However, 3D datasets acquired by transthoracic echocardiography can be analyzed in the same fashion. A major limitation is the missing comparison with RV pressure-volume loops to evaluate the correlations between VSL indices and invasively generated measures. Furthermore, many established echocardiographic parameters, e.g., Doppler-derived indices or diastolic measures, were not systemically available. As the technical nature of the 3D data results in relatively low framerates (~20 to 30 frames per second), a non-inferiority to high-resolution 2D-echocardiography-based area-strain loops remains uncertain. The presented approach is further based on cumbersome data handling and offline analysis, potentially limiting a bedside application in its current form.

Conclusions

Right ventricular volume-strain loop generation from simultaneously recorded volumes and longitudinal and circumferential strains using mesh models derived from three-dimensional STE is feasible. The computed indices

(systolic slopes, systolic intercepts, systolic areas, systolic-diastolic coupling) revealed periprocedural changes of right ventricular contraction in patients undergoing AVS and OPCAB grafting. Whereas non-VSL parameters hinted towards a reduction of predominantly circumferential function, VSL indices potentially indicated reduced RV work while maintaining contractility. Future investigations should focus on the comparison with invasive pressure-volume loops to overcome the main limitations associated with our report. Furthermore, our results require external validation.

Acknowledgments

We thank Tobias Lang for his help and expertise throughout the coding process of the software algorithm.
Funding: This work was supported by Deutsche Forschungsgemeinschaft (DFG) (DFG-INST 2388/71–1 FUGG).

Footnote

Reporting Checklist: The authors have completed the STROBE reporting checklist (available at https://qims.amegroups.com/article/view/10.21037/qims-21-1204/rc).

Conflicts of Interest: All authors have completed the ICMJE uniform disclosure form (available at https://qims.amegroups.com/article/view/10.21037/qims-21-1204/coif). MK and HM report that they have a patent pending on right ventricular 3D mesh-derived volume-strain loop generation. The other authors have no conflicts of interest to declare.

Ethical Statement: The authors are accountable for all aspects of the work in ensuring that questions related to the accuracy or integrity of any part of the work are appropriately investigated and resolved. This study was conducted in accordance with the Declaration of Helsinki (as revised in 2013) and approved by the Ethics Committee of the University of Tuebingen (No. 350/2015R). German privacy regulations do not require individual patient consent for retrospective data acquisition or use.

References

1. Carluccio E, Biagioli P, Alunni G, Murrone A, Zuchi C, Coiro S, Riccini C, Mengoni A, D'Antonio A, Ambrosio G. Prognostic Value of Right Ventricular Dysfunction in Heart Failure With Reduced Ejection Fraction: Superiority of Longitudinal Strain Over Tricuspid Annular Plane Systolic Excursion. Circ Cardiovasc Imaging 2018;11:e006894.
2. Peyrou J, Chauvel C, Pathak A, Simon M, Dehant P, Abergel E. Preoperative right ventricular dysfunction is a strong predictor of 3 years survival after cardiac surgery. Clin Res Cardiol 2017;106:734-42.
3. Bootsma IT, de Lange F, Koopmans M, Haenen J, Boonstra PW, Symersky T, Boerma EC. Right Ventricular Function After Cardiac Surgery Is a Strong Independent Predictor for Long-Term Mortality. J Cardiothorac Vasc Anesth 2017;31:1656-62.
4. Konstam MA, Kiernan MS, Bernstein D, Bozkurt B, Jacob M, Kapur NK, Kociol RD, Lewis EF, Mehra MR, Pagani FD, Raval AN, Ward C; American Heart Association Council on Clinical Cardiology; Council on Cardiovascular Disease in the Young; and Council on Cardiovascular Surgery and Anesthesia. Evaluation and Management of Right-Sided Heart Failure: A Scientific Statement From the American Heart Association. Circulation 2018;137:e578-622.
5. McDonagh TA, Metra M, Adamo M, Gardner RS, Baumbach A, Böhm M, et al. 2021 ESC Guidelines for the diagnosis and treatment of acute and chronic heart failure. Eur Heart J 2021;42:3599-726.
6. van der Zwaan HB, Geleijnse ML, McGhie JS, Boersma E, Helbing WA, Meijboom FJ, Roos-Hesselink JW. Right ventricular quantification in clinical practice: two-dimensional vs. three-dimensional echocardiography compared with cardiac magnetic resonance imaging. Eur J Echocardiogr 2011;12:656-64.
7. Nagata Y, Wu VC, Kado Y, Otani K, Lin FC, Otsuji Y, Negishi K, Takeuchi M. Prognostic Value of Right Ventricular Ejection Fraction Assessed by Transthoracic 3D Echocardiography. Circ Cardiovasc Imaging 2017;10:e005384.

8. Magunia H, Dietrich C, Langer HF, Schibilsky D, Schlensak C, Rosenberger P, Nowak-Machen M. 3D echocardiography derived right ventricular function is associated with right ventricular failure and mid-term survival after left ventricular assist device implantation. Int J Cardiol 2018;272:348-55.
9. Li Y, Wang T, Haines P, Li M, Wu W, Liu M, Chen Y, Jin Q, Xie Y, Wang J, Yang Y, Zhang L, Lv Q, Xie M. Prognostic Value of Right Ventricular Two-Dimensional and Three-Dimensional Speckle-Tracking Strain in Pulmonary Arterial Hypertension: Superiority of Longitudinal Strain over Circumferential and Radial Strain. J Am Soc Echocardiogr 2020;33:985-994.e1.
10. Smith BC, Dobson G, Dawson D, Charalampopoulos A, Grapsa J, Nihoyannopoulos P. Three-dimensional speckle tracking of the right ventricle: toward optimal quantification of right ventricular dysfunction in pulmonary hypertension. J Am Coll Cardiol 2014;64:41-51.
11. Vonk-Noordegraaf A, Westerhof N. Describing right ventricular function. Eur Respir J 2013;41:1419-23.
12. Chen Y, Shlofmitz E, Khalid N, Bernardo NL, Ben-Dor I, Weintraub WS, Waksman R. Right Heart Catheterization-Related Complications: A Review of the Literature and Best Practices. Cardiol Rev 2020;28:36-41.
13. Gufler H, Wagner S, Niefeldt S, Klopsch C, Brill R, Wohlgemuth WA, Yerebakan C. Levels of agreement between cardiac magnetic resonance and conductance catheter measurements of right ventricular volumes after pulmonary artery banding. Acta Radiol 2020;61:894-902.
14. Tello K, Dalmer A, Vanderpool R, Ghofrani HA, Naeije R, Roller F, Seeger W, Wilhelm J, Gall H, Richter MJ. Cardiac Magnetic Resonance Imaging-Based Right Ventricular Strain Analysis for Assessment of Coupling and Diastolic Function in Pulmonary Hypertension. JACC Cardiovasc Imaging 2019;12:2155-64.
15. Axell RG, Giblett JP, White PA, Klein A, Hampton-Til J, O'Sullivan M, Braganza D, Davies WR, West NEJ, Densem CG, Hoole SP. Stunning and Right Ventricular Dysfunction Is Induced by Coronary Balloon Occlusion and Rapid Pacing in Humans: Insights From Right Ventricular Conductance Catheter Studies. J Am Heart Assoc 2017;6:005820.
16. Kleinnibbelink G, Hulshof HG, van Dijk APJ, Ten Cate T, George KP, Oxborough DL, Thijssen DHJ. Effects of Preload Manipulation on Right Ventricular Contractility: Invasive Pressure-Area Loop versus Non-invasive Strain-Area Loop. J Am Soc Echocardiogr 2021;34:447-9.
17. Oxborough D, Heemels A, Somauroo J, McClean G, Mistry P, Lord R, Utomi V, Jones N, Thijssen D, Sharma S, Osborne R, Sculthorpe N, George K. Left and right ventricular longitudinal strain-volume/area relationships in elite athletes. Int J Cardiovasc Imaging 2016;32:1199-211.
18. Hulshof HG, van Dijk AP, Hopman MTE, Heesakkers H, George KP, Oxborough DL, Thijssen DHJ. 5-Year prognostic value of the right ventricular strain-area loop in patients with pulmonary hypertension. Eur Heart J Cardiovasc Imaging 2021;22:188-95.
19. Keller M, Heller T, Lang T, Patzelt J, Schreieck J, Schlensak C, Rosenberger P, Magunia H. Acute changes of global and longitudinal right ventricular function: an exploratory analysis in patients undergoing open-chest mitral valve surgery, percutaneous mitral valve repair and off-pump coronary artery bypass grafting. Cardiovasc Ultrasound 2020;18:32.
20. Nowak-Machen M, Lang T, Schilling A, Mockenhaupt L, Keller M, Rosenberger P, Magunia H. Regional Right Ventricular Volume and Function Analysis Using Intraoperative 3-Dimensional Echocardiography-Derived Mesh Models. J Cardiothorac Vasc Anesth 2019;33:1527-32.
21. Magunia H, Jordanow A, Keller M, Rosenberger P, Nowak-Machen M. The effects of anesthesia induction and positive pressure ventilation on right-ventricular function: an echocardiography-based prospective observational study. BMC Anesthesiol 2019;19:199.
22. Keller M, Lang T, Schilling A, Nowak-Machen M, Rosenberger P, Magunia H. Novel mesh-derived right ventricular free wall longitudinal strain analysis by intraoperative three-dimensional transoesophageal speckle-tracking echocardiography: a comparison with conventional parameters. Int J Cardiovasc Imaging 2019;35:2177-88.
23. Keller M, Heller T, Duerr MM, Schlensak C, Nowak-Machen M, Feng YS, Rosenberger P, Magunia H. Association of Three-Dimensional Mesh-Derived Right Ventricular Strain with Short-Term Outcomes in Patients Undergoing Cardiac Surgery. J Am Soc Echocardiogr 2022;35:408-18.
24. Tokodi M, Németh E, Lakatos BK, Kispál E, Tősér Z, Staub L, Rácz K, Soltész Á, Szigeti S, Varga T, Gál J, Merkely B, Kovács A. Right ventricular mechanical pattern in patients undergoing mitral valve surgery: a predictor of post-operative dysfunction? ESC Heart Fail 2020;7:1246-56.
25. Singh A, Huang X, Dai L, Wyler D, Alfirevic A, Blackstone EH, Pettersson GB, Duncan AE. Right

ventricular function is reduced during cardiac surgery independent of procedural characteristics, reoperative status, or pericardiotomy. J Thorac Cardiovasc Surg 2020;159:1430-1438.e4.
26. Keyl C, Schneider J, Beyersdorf F, Ruile P, Siepe M, Pioch K, Schneider R, Jander N. Right ventricular function after aortic valve replacement: a pilot study comparing surgical and transcatheter procedures using 3D echocardiography. Eur J Cardiothorac Surg 2016;49:966-71.
27. Raina A, Vaidya A, Gertz ZM, Susan Chambers, Forfia PR. Marked changes in right ventricular contractile pattern after cardiothoracic surgery: implications for post-surgical assessment of right ventricular function. J Heart Lung Transplant 2013;32:777-83.
28. de Waal EE, De Boeck BW, Kruitwagen CL, Cramer MJ, Buhre WF. Effects of on-pump and off-pump coronary artery bypass grafting on left ventricular relaxation and compliance: a comprehensive perioperative echocardiography study. Eur J Echocardiogr 2010;11:732-7.
29. McKenney PA, Apstein CS, Mendes LA, Connelly GP, Aldea GS, Shemin RJ, Davidoff R. Increased left ventricular diastolic chamber stiffness immediately after coronary artery bypass surgery. J Am Coll Cardiol 1994;24:1189-94.
30. Ashes CM, Yu M, Meineri M, Katznelson R, Carroll J, Rao V, Djaiani G. Diastolic dysfunction, cardiopulmonary bypass, and atrial fibrillation after coronary artery bypass graft surgery. Br J Anaesth 2014;113:815-21.
31. Moya Mur JL, García Martín A, García Lledó A, Lázaro Rivera C, Rincón Díaz LM, Miguelena Hycka J, Boretti I, Gimaraes C, Casas Rojo E, Jiménez Nacher JJ, Fernández-Golfín C, Rodríguez-Roda Stuart J, Zamorano JL. Geometrical and functional cardiac changes after cardiac surgery: a phisiopatological explanation based on speckle tracking. Int J Cardiovasc Imaging 2018;34:1905-15.
32. Donauer M, Schneider J, Jander N, Beyersdorf F, Keyl C. Perioperative Changes of Right Ventricular Function in Cardiac Surgical Patients Assessed by Myocardial Deformation Analysis and 3-Dimensional Echocardiography. J Cardiothorac Vasc Anesth 2020;34:708-18.
33. Labus J, Winata J, Schmidt T, Nicolai J, Tomko M, Sveric K, Wilbring M, Fassl J. Perioperative Course of Three-Dimensional-Derived Right Ventricular Strain in Coronary Artery Bypass Surgery: A Prospective, Observational, Pilot Trial. J Cardiothorac Vasc Anesth 2021;35:1628-37.
34. Lakatos BK, Nabeshima Y, Tokodi M, Nagata Y, Tősér Z, Otani K, Kitano T, Fábián A, Ujvári A, Boros AM, Merkely B, Kovács A, Takeuchi M. Importance of Nonlongitudinal Motion Components in Right Ventricular Function: Three-Dimensional Echocardiographic Study in Healthy Volunteers. J Am Soc Echocardiogr 2020;33:995-1005.e1.
35. Hulshof HG, van Dijk AP, George KP, Merkus D, Stam K, van Duin RW, van Tertholen K, Hopman MTE, Haddad F, Thijssen DHJ, Oxborough DL. Echocardiographic-Derived Strain-Area Loop of the Right Ventricle is Related to Pulmonary Vascular Resistance in Pulmonary Arterial Hypertension. JACC Cardiovasc Imaging 2017;10:1286-8.
36. Butcher SC, Fortuni F, Montero-Cabezas JM, Abou R, El Mahdiui M, van der Bijl P, van der Velde ET, Ajmone Marsan N, Bax JJ, Delgado V. Right ventricular myocardial work: proof-of-concept for non-invasive assessment of right ventricular function. Eur Heart J Cardiovasc Imaging 2021;22:142-52.

Cite this article as: Keller M, Puhlmann AS, Heller T, Rosenberger P, Magunia H. Right ventricular volume-strain loops using 3D echocardiography-derived mesh models: proof-of-concept application on patients undergoing different types of open-heart surgery. Quant Imaging Med Surg 2022;12(7):3679-3691. doi: 10.21037/qims-21-1204

